3D-mapping of human lymph node and spleen reveals integrated neuronal, vascular, and ductal cell networks

Seth Currlin[1,2], Harry S. Nick[1], Marda Jorgensen[3], Jerelyn A. Nick[3], Maigan A. Brusko[3], Hunter Hakimian[2], Jesus Penaloza-Aponte[3], Natalie Rodriguez[3], Miguel Medina-Serpas[3], Mingder Yang[3], Irina Kusmartseva[3], Todd M. Brusko[3,4], Kevin Otto[2], Amanda L. Posgai[3], Clive H. Wasserfall[3], Mark A. Atkinson[3,4]*

[1]Department of Neuroscience, College of Medicine, University of Florida, 1149 Newell Drive, Room L1-100, Gainesville, FL 32601.

[2]J. Crayton Pruitt Family Department of Biomedical Engineering, Herbert Wertheim College of Engineering, University of Florida, 1275 Center Drive, Biomedical Sciences Building, 3rd Floor, Gainesville, FL 32611.

[3]Department of Pathology, Immunology, and Laboratory Medicine, Diabetes Institute, College of Medicine, University of Florida, 1275 Center Drive, Biomedical Sciences Building, 5th Floor, Gainesville, FL 32611.

[4]Department of Pediatrics, College of Medicine, University of Florida, 1600 SW Archer Road, Gainesville, FL 32610.

Words: 2,558

Display items: 5 Figures

References: 48

Methods References: 1

Extended Data: 9 Figures, 1 Table

Supplementary Information: 6 Movies, 1 Table

Abstract

As secondary lymphoid organs, the spleen and lymph node represent important hubs for both innate and adaptive immunity[1,2]. Neuroanatomical and tracing data, largely derived from rodents, suggest that lymph nodes contain sensory and sympathetic innervation[3,4], whereas the spleen contains postganglionic sympathetic innervation[5], with conflicting views regarding the existence of cholinergic or vagal innervation[6]. Herein, we map the neuronal, vascular, and sinus cell networks from human spleen and lymph node using highly multiplexed CODEX (CO-Detection by indEXing) and 3D light sheet microscopy of cleared tissues. These data demonstrate striking delineation of two distinct layers within the lymph node subcapsular sinus—the ceiling defined by Podoplanin expression and floor by LYVE1, which overlays the lymph node follicles. Within the lymph node interior, we observed a mesh-like vessel network innervated with GAP43 and β3-tubulin. Dense perivascular innervation occurred in both tissues, including a subset of axonal processes expressing choline acetyl transferase (ChAT). Four neuronal markers (ChAT, PGP9.5, tyrosine hydroxylase, and β3-tubulin) localized to the arterial *tunica externa* suggest expression in the *nervi vasorum* while GAP43 was expressed within the internal elastic membrane of arteries. These data represent highly novel 3D visualization of perivascular and periductal autonomic innervation within these two key human organs.

Main

With similarities to the circulation, the organization and function of the lymphatic system stretches across the entire human body[7,8]. It is critical in conducting lymphatic fluid, blood filtration, mounting defenses against infections and cancer, as well as regulating immune cells to protect against autoimmune diseases[7,8]. Tissue organization and function are directly linked in spleen (SPL; blood filtration) and lymph nodes (LN; interstitial fluid filtration) facilitating immune cell priming and activation for peripheral immunity[8]. The autonomic nervous system provides control of host immune defense mechanisms through innervation from sympathetic postganglionic neurons, specifically the splenic nerve for the SPL and anatomically paired nerve fibers for respective LNs[9]. However, much of our knowledge regarding the architecture and function of the lymphatic system derives from rodents[10], with recent studies noting a series of key architectural differences compared to humans[11,12].

Indeed, recent 3D imaging and topological mapping of the murine LN[13,14], using methods independent of protein markers and cell types, have described a mesh-like network composed of fibroblastic reticular cells (FRCs) that provide the homing zone for T cells and may mediate B cell homeostasis[15]. Moreover, Huang and colleagues recently demonstrated the murine LN capsule to be encased by a network of sensory neurons capable of neuroimmune transcriptional regulation[16]. The delivery of antigens[17], inflammatory mediators, and even larger molecules[18] to the LN T cell zone involves the transport of lymph initially filtered through the subcapsular sinus, followed by transport among an elaborate conduit system of lymphatic micro-vessels. Similarly, Ogembo et al.[12] and originally Buckley et al.[19] have elegantly described SIRPα, FHOD1, HLA-DR, CD36 (platelet glycoprotein IV), CD71 (transferrin receptor), CD4, and CD8α as cell markers expressed by the littoral cells (LC) lining the splenic sinusoids. LC exist exclusively in human SPL and are not observed in rodents or even non-human primates[12,19]. However, human tissue studies have historically been limited to single or two-dimensional (2D) tissue cross-

sections stained for low-parameter combinations of markers, highlighting the need to characterize the human SPL and LN using highly multiplexed and three-dimensional (3D) modalities.

Detection of immune markers in human SPL and LN

To extensively profile the cellular architecture of the lymphatic endothelial cells, blood vessels, and innervation within the human SPL and LN, tissues were acquired from seven non-diseased organ donors (Extended Data Table 1) through the Human BioMolecular Atlas Program (HuBMAP)[20] Lymphatic System Tissue Mapping Center (TMC) at the University of Florida. SPL and LN tissues were obtained from organ donors through a nationwide organ procurement network. Cases were selected based on criteria (https://www.protocols.io/view/donor-acceptance-criteria-for-tmc-florida-zurich-h-bipykdpw) of healthy general population without documented major inherent pathologies with tissue "normality" confirmed by an independent pathologist. All antibodies used in this study were first validated by immunohistochemistry (IHC), illustrating the expected organ-specific staining patterns within formalin fixed paraffin embedded (FFPE) tissue sections (Extended Data Fig. 1). SPL and LN tissue sections were then stained with a 28-marker panel (Supplemental Table 1) for highly multiplexed imaging using CODEX (CO-Detection by indexing), which employs detection via repeated oligonucleotide exchange reaction[21,22]. Visualizing the expression patterns for a subset of immune markers [B cell (CD20), T cell (CD3ε, CD4, CD8α), neutrophil (CD15), and macrophage/Dendritic cell (CD68); Extended Data Fig. 2] further validated the organ-specific architecture composed of repeating functional units (i.e., follicles), and also highlighted differences in the antigen distributions within these two immune organs. The complete dataset with all 28 markers was made available on the HuBMAP data portal (https://portal.hubmapconsortium.org/search?entity_type[0]=Dataset).

2D-imaging of lymphatic and blood vessels in human SPL and LN by CODEX

In an effort to map the innervation of lymphatic and blood endothelial cells (LECs and BECs, respectively) within human SPL and LN, we utilized CODEX to visualize associated markers discriminating endothelial cell subtypes[23,24]. These include LYVE1, podoplanin (PDPN), and PROX1 for LECs[25] as well as CD31[26] and CD34[27] for BECs. Our results demonstrate that LYVE1 and PDPN expression do not overlap either in the LN or SPL (Fig. 1). Furthermore, PDPN and LYVE1 appear to define the ceiling and floor of the LN subcapsular sinus[25] (SCS), respectively, as depicted in Fig. 1a-d and annotated in Extended Data Fig. 3. PDPN$^+$ cells are also observed within the follicles, surrounding large arteries, and defining the thin wall of afferent or efferent lymphatic vessels of the LN (Fig. 1b-d; Extended Data Fig. 4a-c). LN arteries expressing both CD31 and CD34, as well as CD34$^+$ vessels were identified in the capsule and ceiling of the SCS and were surrounded by PDPN$^+$ and smooth muscle actin (SMA)-expressing cells (Fig. 1a-d). These data also demonstrate CD31$^+$ cells localizing adjacent to LYVE1$^+$ LECs in the SCS floor, contrasting with CD34 occupancy in the PDPN$^+$ SCS ceiling (Fig.1a-c). Large clusters of LYVE1$^+$ endothelial cells throughout the LN (Fig. 1d) mark lymphatic sinuses[13,14] of the cortex and medulla. This observation is supported with a third LEC marker, a homeobox transcription factor (PROX1)[28], marking LEC nuclei within LYVE1$^+$ sinuses (Extended Data Fig. 4d). Additionally, the lumen of LN lymphatic vessel cross-sections can be appreciated when LYVE1 is overlaid with DAPI staining for nuclei (Extended Data Fig. 4d, far right panel). Similar to LN, expression of LYVE1 and PDPN does not overlap in the spleen, with PDPN present within follicles and defining central arteries of follicles (Fig. 1e). Strikingly, LYVE1$^+$ cells throughout the spleen clearly define the extensive network of splenic venous sinuses (Fig. 1e). To corroborate the representative images in Fig. 1, we provide additional CODEX datasets both from independent donors and from within multiple common coordinate framework (CCF)[29,30]-defined tissue regions for both LN and SPL (Extended Data Fig. 4 and 5).

Fig 2a and b further demonstrate that LYVE1 labels the LN lymphatic medullary sinus system[14] and SPL venous sinuses[31]. Vimentin expression is observed throughout LYVE1

vessels in the LN medullary sinus system (Fig. 2a), while overlapping with LYVE1 specifically in human splenic sinusoidal LCs[12] (Fig. 2b). To extend these unique observations, we provide supporting evidence with multiplex images in both LN and SPL comparing LYVE1 expression patterns with additional markers (CD8α, CD107a, and CD163). The CD8αβ heterodimer is a canonical marker for cytotoxic T cells[32], and as expected, CD8α labels individual cells scattered across the LN (Fig. 2a). However, within the SPL, CD8α labels scattered cells but also defines LCs, as originally documented by Ogembo et al.[12]. Indeed, our data demonstrate that CD8α overlaps with LYVE1 within the splenic LC (Fig. 2b). Similarly, CD107a [lysosome-associated membrane glycoprotein 1 (LAMP-1)] is classically associated with cytotoxic degranulation in Natural Killer (NK) and CD8 T cells[33] as well as leukocyte adhesion to the vascular endothelium[34]. Within the two tissues examined, CD107a was observed throughout the vessels of the LN medullary sinus network (Fig. 2c), scattered across the SPL, and outlining the splenic venous sinuses overlapping with LYVE1 (Fig. 2d). Within the LN, the macrophage marker CD163 associates with LYVE1^{+} lymphatic medullary sinuses (Fig. 2c) while in the SPL, CD163 interdigitates between venous sinuses— identified by LYVE1, vimentin and CD8α— within the red pulp (Fig. 2d). We also provide corroborating images from independent organs for these markers for both LN (Extended Data Fig. 6) and SPL (Extended Data Fig. 7). These 2D CODEX data form the basis for 3D visualization of innervation in these secondary lymphatic organs using multicolor light sheet fluorescence microscopy (LSFM).

3D-imaging of perivascular innervation in SPL and LN

To visualize vascular innervation of the human LN and SPL in 3D, we employed three-color LSFM[35,36] on tissues cleared using CLARITY-based methodology[37,38]. Extensive 3D perivascular innervation was observed on CD31^{+} endothelial cells within vessels of human LN (Fig. 3a-d) and SPL (Fig. 3e-h). CD31 specificity was strikingly visualized at the individual endothelial cell

level in the SPL (Extended Data Fig. 8a). Staining with the pan-neuronal marker PGP9.5 revealed a complex matrix of neural processes surrounding $CD31^+$ vasculature of the LN (Fig. 3b,c) and SPL (Fig. 3f-g) located within the *nervi vasorum* of the *tunica externa* layer of the vessel wall (Fig. 3d and 3h, respectively). *Nervi vasorum* staining was also observed in SPL for the peripheral sympathetic neuronal marker tyrosine hydroxylase (TH) (Extended Data Fig. 8b, Supplemental Movie 1). Interestingly, choline acetyltransferase (ChAT), an enzyme required for production of the neurotransmitter acetylcholine within parasympathetic neurons, co-localizes with unique segments of the $PGP9.5^+$ perivascular neural matrix in the LN (Fig. 3c) and SPL (Fig. 3f-g, Extended Data Fig. 8c). This is in contrast with longstanding dogma[39] as well as a recent 3D imaging study of cleared SPL from mice where $ChAT^+$ nerve fibers were not detected[40]. Renderings of sequential optical slices through the Z dimension (~1000-2000) provide further 3D visualization of perivascular innervation within LN (Supplemental Movie 2) and SPL (Supplemental Movie 3) demonstrating that PGP9.5, ChAT, and TH primarily label neuronal processes on larger blood vessels in both organs.

In stark contrast with PGP9.5, ChAT, and TH, 3D LSFM studies of LN innervation with the pan-neuronal marker β3-tubulin and neuronal growth-associated protein (GAP43, or neuromodulin) revealed the extensive mesh-like network[13,14] (Fig. 4a-c; Supplemental Movie 4) putatively corresponding to the lymphatic conduit system (Fig 1a-d and Extended Data Fig. 4). β3-tubulin is also observed in axon bundles adjacent to blood vessels (Fig. 4b; Supplemental Movie 5), as well as in the *nervi vasorum* of vessel walls (Fig. 4d), much like TH and ChAT (Fig. 3).

As expected, the leukocyte marker, Coronin-1A, was detected throughout the LN (Fig. 4a,c; Supplemental Movie 5) and localized to cell membranes (Fig. 4b, right). In the SPL, Coronin-1A displayed a less homogenous distribution, with expression observed on randomly distributed single cells and on cells clustered around large vascular structures innervated by β3-tubulin (Fig. 4e). Within the SPL β3-tubulin identifies large vascular structures whereas GAP43

identifies both large and small vessels (Fig. 4e-h), corresponding either to BEC or efferent LECs since the spleen lacks afferent LECs[41]. Surprisingly, immunolabeling with GAP43 demonstrated strong staining also localized to the internal elastic membrane or smooth muscle layer of large blood vessels in both LN (Fig. 4d) and SPL (Fig. 4i). These GAP43 data clearly define filamentous neuronal processes existing on the internal aspect of large vessels, unexpected from conventional *nervi vasorum* location of vascular innervation. To our knowledge, this localization of GAP43 expressing neurons has not previously been reported in human LN or SPL vessels. These novel findings are further summarized in Extended Data Fig. 8d.

Differential expression of perivascular GAP43 and β3-tubulin in LN and SPL

While large blood vessel innervation was identified by both β3-tubulin and GAP43 expression, a detailed review of our 3D LSFM data revealed a novel observation involving differential expression of these markers along discrete segments of large vessels in both organs (Fig. 5 and Extended Data Fig. 9). Specifically within LN, select segments of large vessels displayed a reduction or absence of protein expression for either GAP43 (Fig. 5a,e) or β3-tubulin (Fig. 5b-d,f). Similarly, GAP43 protein expression was significantly diminished along segments of certain large vessels within the SPL relative to robust expression of β3-tubulin (Fig. 5g-i, two left-most panels). Figure 5g also reaffirms the observation that within the SPL, GAP43 detects neuronal processes on both large and small vessels, while the pan-neuronal marker β3-tubulin is primarily found on cells along large vessels (Fig. 4e-h). Remarkably, our multiplexed 3D LSFM strategy revealed that the diminished expression of GAP43 along segments of large vessels in the SPL is consistently associated with a locally concentrated population of Coronin-1A^{+} immune cells (Fig. 5g-i, two right-most panels; Supplemental Movie 6).

Discussion

Herein we provide novel 2D and 3D characterization of the lymphatic, vascular, and neuronal cellular networks within the normal human LN and SPL. Among key observations, LYVE1 and PDPN do not overlap in LN or SPL. While ACKR4^{+}NT5E^{+}Caveolin-1^{+} cells and TNFRSF9^{+}CCK20^{+}CXCL1^{-}CXCL5^{+} have been proposed to delineate the LN subcapsular sinus floor and ceiling, respectively[25], we posit that LYVE1 and PDPN serve the purpose to demarcate these anatomical features as well as the mesh-like clusters of lymphatic sinuses throughout the LN interior. Indeed, we observed a striking separation of LYVE1 and PDPN expression in LN, shedding new light upon recent studies that applied PDPN^{+} cell sorting to isolate LEC prior to single cell transcriptomics[42,43]. This carries too for the SPL data presented herein, which similarly demonstrated strong separation of PDPN and LYVE1 expression. Furthermore, observations of strong PDPN expression in SPL trabecula, follicles, and central arterioles, conflict with reports that CD31^{+}PDPN^{+} FRCs are restricted to T cell zones[44]. Finally, LYVE1 defines an extensive network of splenic venous sinuses that also express vimentin, CD8α, and CD107a, likely reflecting LCs, which are responsible for red blood cell turnover. LCs do not exist in rodents or non-human primates, emphasizing the importance of performing these cell mapping studies in human tissue[12].

Our data highlight the power and utility of 3D image analysis: the ability to observe volumetric data, consisting of thousands of optical sections from any vantage. This enables unique insights into human tissue organization that may be masked by other visualization modes, such as max projection or single-section 2D views. Moreover, given HuBMAP's use of a CCF, the images presented herein can be mapped back to their physical location within the intact organ. By applying three-color immunofluorescent staining to cleared 3D tissue volumes, this effort represents an advance on prior LSFM imaging studies. Within both LN and SPL, the PGP9.5, β3-tubulin, ChAT, and TH neuronal markers identify extensive perivascular neuronal

processes localized to the *nervi vasorum* of the *tunica externa*, while GAP43 appears to localize to the internal elastic membrane or smooth muscle layers of the artery, suggesting that there are neuronal processes internal to the *tunica externa* defined by GAP43[45]. We further observed that GAP43 and β3-tubulin identify an extensive network of small vessels within the LN. Moving forward, there is a need to corroborate our interpretation that LN LYVE1 staining, visualized in 2D via CODEX, corresponds with the 3D mesh-like sinus vessel network, which we visualized as being heavily innervated by β3-tubulin and GAP43 expressing neurons. Within the LN, β3-tubulin also identified axon bundles adjacent to vasculature.

Within the SPL and LN, the leukocyte marker, Coronin-1A, identifies scattered single cells and clusters of leukocytes focused around vascular structures. However, within the SPL, accumulation of leukocytes in close juxtaposition to blood vessels was associated with dramatically reduced expression of GAP43 within the *tunica media* or *tunica intima*. Future work will require functional assays to determine if GAP43 negative regions correspond to sites of immune cell extravasation and navigation[46], potentially regulated by a splenic neurovascular unit[47].

The data presented herein highlight key anatomical differences between rodent and human tissues as well as showcase differential staining patterns of lymphatic, vascular, immune, and neural markers within secondary lymphoid organs, underscoring the need to extend these studies to understand neuronal control of lymphatic connections across tissues throughout the human body. Given that most human immune responses occur in secondary lymphatics and not peripheral blood[48], there is a clear need for additional insights on how these integrated nerve, vascular and ductal cell networks interact, modulating immune activity across the lymphatic system, including within all organs, in humans. Importantly, the current 3D cell mapping effort sets the stage for future studies to determine how these pathways may be dysregulated in various disease settings, including autoimmunity, sepsis, cancer, and COVID-

19. We envision that novel therapies targeting the neurovascular sites mapped herein could potentially be developed to specifically modulate immune function within the human SPL and LN. The HuBMAP Consortium[20] provides an invaluable resource to address these questions.

Main References

1 Krishnamurty, A. & Turley, S. Lymph node stromal cells: cartographers of the immune system. *Nature Immunology* **21**, 369-380, doi:10.1038/s41590-020-0635-3 (2020).

2 Bronte, V. & Pittet, M. The spleen in local and systemic regulation of immunity. *Immunity* **39**, 806-818, doi:10.1016/j.immuni.2013.10.010 (2013).

3 Wang, P., Czepielewski, R. & Randolph, G. Sensory Nerves Regulate Transcriptional Dynamics of Lymph Node Cells. *Trends in Immunology* **42**, 180-182, doi:10.1016/j.it.2021.01.008 (2021).

4 Felten, D. *et al.* Sympathetic innervation of lymph nodes in mice. *Brain Research Bulletin* **13**, 693-699, doi:10.1016/0361-9230(84)90230-2 (1984).

5 Murray, K. *et al.* Neuroanatomy of the spleen: Mapping the relationship between sympathetic neurons and lymphocytes. *PLoS One* **12**, e0182416, doi:10.1371/journal.pone.0182416 (2017).

6 Anderson, C., McKinley, M., Martelli, D. & McAllen, R. Letter to the editor: Parasympathetic innervation of the rodent spleen? *Am J Physiol Heart Circ Physiol* **309**, H2158, doi:10.1152/ajpheart.00766.2015 (2015).

7 Betterman, K. L. & Harvey, N. L. The lymphatic vasculature: development and role in shaping immunity. *Immunol Rev* **271**, 276-292, doi:10.1111/imr.12413 (2016).

8 Randolph, G. J., Ivanov, S., Zinselmeyer, B. H. & Scallan, J. P. The Lymphatic System: Integral Roles in Immunity. *Annu Rev Immunol* **35**, 31-52, doi:10.1146/annurev-immunol-041015-055354 (2017).

9 Bachmann, S. B. *et al.* A Distinct Role of the Autonomic Nervous System in Modulating the Function of Lymphatic Vessels under Physiological and Tumor-Draining Conditions. *Cell Rep* **27**, 3305-3314 e3313, doi:10.1016/j.celrep.2019.05.050 (2019).

10 Xiang, M. *et al.* A Single-Cell Transcriptional Roadmap of the Mouse and Human Lymph Node Lymphatic Vasculature. *Front Cardiovasc Med* **7**, 52, doi:10.3389/fcvm.2020.00052 (2020).

11 Steiniger, B., Timphus, E. M. & Barth, P. J. The splenic marginal zone in humans and rodents: an enigmatic compartment and its inhabitants. *Histochem Cell Biol* **126**, 641-648, doi:10.1007/s00418-006-0210-5 (2006).

12 Ogembo, J. G. *et al.* SIRPalpha/CD172a and FHOD1 are unique markers of littoral cells, a recently evolved major cell population of red pulp of human spleen. *J Immunol* **188**, 4496-4505, doi:10.4049/jimmunol.1103086 (2012).

13 Kelch, I. D. *et al.* High-resolution 3D imaging and topological mapping of the lymph node conduit system. *PLoS Biol* **17**, e3000486, doi:10.1371/journal.pbio.3000486 (2019).

14 Novkovic, M., Onder, L., Bocharov, G. & Ludewig, B. Topological Structure and Robustness of the Lymph Node Conduit System. *Cell Rep* **30**, 893-904 e896, doi:10.1016/j.celrep.2019.12.070 (2020).

15 Fletcher, A., Acton, S. & Knoblich, K. Lymph node fibroblastic reticular cells in health and disease. *Nature Reviews Immunology* **15**, 350-361, doi:10.1038/nri3846 (2015).

16 Huang, S. *et al.* Lymph nodes are innervated by a unique population of sensory neurons with immunomodulatory potential. *Cell* **184**, 441-459.e425, doi:10.1016/j.cell.2020.11.028 (2021).

17 Sixt, M. *et al.* The conduit system transports soluble antigens from the afferent lymph to resident dendritic cells in the T cell area of the lymph node. *Immunity* **22**, 19-29, doi:10.1016/j.immuni.2004.11.013 (2005).

18 Reynoso, G. V. *et al.* Lymph node conduits transport virions for rapid T cell activation. *Nat Immunol* **20**, 602-612, doi:10.1038/s41590-019-0342-0 (2019).

19 Buckley, P. J., Dickson, S. A. & Walker, W. S. Human splenic sinusoidal lining cells express antigens associated with monocytes, macrophages, endothelial cells, and T lymphocytes. *J Immunol* **134**, 2310-2315 (1985).
20 HuBMAP Consortium. The human body at cellular resolution: the NIH Human Biomolecular Atlas Program. *Nature* **574**, 187-192, doi:10.1038/s41586-019-1629-x (2019).
21 Goltsev, Y. *et al.* Deep Profiling of Mouse Splenic Architecture with CODEX Multiplexed Imaging. *Cell* **174**, 968-981 e915, doi:10.1016/j.cell.2018.07.010 (2018).
22 Schurch, C. M. *et al.* Coordinated Cellular Neighborhoods Orchestrate Antitumoral Immunity at the Colorectal Cancer Invasive Front. *Cell* **182**, 1341-1359 e1319, doi:10.1016/j.cell.2020.07.005 (2020).
23 Kong, L. L. *et al.* The optimum marker for the detection of lymphatic vessels. *Mol Clin Oncol* **7**, 515-520, doi:10.3892/mco.2017.1356 (2017).
24 Ribatti, D., Tamma, R., Ruggieri, S., Annese, T. & Crivellato, E. Surface markers: An identity card of endothelial cells. *Microcirculation* **27**, e12587, doi:10.1111/micc.12587 (2020).
25 Jalkanen, S. & Salmi, M. Lymphatic endothelial cells of the lymph node. *Nat Rev Immunol* **20**, 566-578, doi:10.1038/s41577-020-0281-x (2020).
26 Lertkiatmongkol, P., Liao, D., Mei, H., Hu, Y. & Newman, P. J. Endothelial functions of platelet/endothelial cell adhesion molecule-1 (CD31). *Curr Opin Hematol* **23**, 253-259, doi:10.1097/MOH.0000000000000239 (2016).
27 Fina, L. *et al.* Expression of the CD34 gene in vascular endothelial cells. *Blood* **75**, 2417-2426 (1990).
28 Oliver, G. Lymphatic vasculature development. *Nature Reviews Immunology* **4**, 35-45, doi:10.1038/nri1258 (2004).
29 Rood, J. *et al.* Toward a Common Coordinate Framework for the Human Body. *Cell* **179**, 1455-1467, doi:10.1016/j.cell.2019.11.019 (2019).
30 Weber, G., Ju, Y. & Börner, K. Considerations for Using the Vasculature as a Coordinate System to Map All the Cells in the Human Body. *Frontiers in Cardiovascular Medicine* **7**, 29, doi:10.3389/fcvm.2020.00029 (2020).
31 Steiniger, B., Stachniss, V., Schwarzbach, H. & Barth, P. J. Phenotypic differences between red pulp capillary and sinusoidal endothelia help localizing the open splenic circulation in humans. *Histochem Cell Biol* **128**, 391-398, doi:10.1007/s00418-007-0320-8 (2007).
32 Reina-Campos, M., Scharping, N. E. & Goldrath, A. W. CD8(+) T cell metabolism in infection and cancer. *Nat Rev Immunol*, doi:10.1038/s41577-021-00537-8 (2021).
33 Aktas, E., Kucuksezer, U., Bilgic, S., Erten, G. & Deniz, G. Relationship between CD107a expression and cytotoxic activity. *Cellular Immunology* **254**, 149-154, doi:10.1016/j.cellimm.2008.08.007 (2009).
34 Kannan, K. *et al.* Lysosome-associated membrane proteins h-LAMP1 (CD107a) and h-LAMP2 (CD107b) are activation-dependent cell surface glycoproteins in human peripheral blood mononuclear cells which mediate cell adhesion to vascular endothelium. *Cellular Immunology* **171**, 10-19, doi:10.1006/cimm.1996.0167 (1996).
35 Power, R. M. & Huisken, J. A guide to light-sheet fluorescence microscopy for multiscale imaging. *Nat Methods* **14**, 360-373, doi:10.1038/nmeth.4224 (2017).
36 Wan, Y., McDole, K. & Keller, P. J. Light-Sheet Microscopy and Its Potential for Understanding Developmental Processes. *Annu Rev Cell Dev Biol* **35**, 655-681, doi:10.1146/annurev-cellbio-100818-125311 (2019).
37 Chung, K. *et al.* Structural and molecular interrogation of intact biological systems. *Nature* **497**, 332-337, doi:10.1038/nature12107 (2013).

38 Gradinaru, V., Treweek, J., Overton, K. & Deisseroth, K. Hydrogel-Tissue Chemistry: Principles and Applications. *Annu Rev Biophys* **47**, 355-376, doi:10.1146/annurev-biophys-070317-032905 (2018).

39 Nance, D. & Sanders, V. Autonomic innervation and regulation of the immune system (1987-2007). *Brain, Behavior, and Immunity* **21**, 736-745, doi:10.1016/j.bbi.2007.03.008 (2007).

40 Ding, X. *et al.* Panicle-Shaped Sympathetic Architecture in the Spleen Parenchyma Modulates Antibacterial Innate Immunity. *Cell Reports* **27**, 3799-3807.e3793, doi:10.1016/j.celrep.2019.05.082 (2019).

41 Mebius, R. E. & Kraal, G. Structure and function of the spleen. *Nat Rev Immunol* **5**, 606-616, doi:10.1038/nri1669 (2005).

42 Berendam, S. *et al.* Comparative Transcriptomic Analysis Identifies a Range of Immunologically Related Functional Elaborations of Lymph Node Associated Lymphatic and Blood Endothelial Cells. *Frontiers in Immunology* **10**, 816, doi:10.3389/fimmu.2019.00816 (2019).

43 Fujimoto, N. *et al.* Single-cell mapping reveals new markers and functions of lymphatic endothelial cells in lymph nodes. *PLoS Biology* **18**, e3000704, doi:10.1371/journal.pbio.3000704 (2020).

44 Scandella, E. *et al.* Restoration of lymphoid organ integrity through the interaction of lymphoid tissue-inducer cells with stroma of the T cell zone. *Nature Immunology* **9**, 667-675, doi:10.1038/ni.1605 (2008).

45 Yang, H., Wang, L., Huang, C. & Ju, G. Plasticity of GAP-43 innervation of the spleen during immune response in the mouse. Evidence for axonal sprouting and redistribution of the nerve fibers. *Neuroimmunomodulation* **5**, 53-60, doi:10.1159/000026326 (1998).

46 Stark, K. *et al.* Capillary and arteriolar pericytes attract innate leukocytes exiting through venules and 'instruct' them with pattern-recognition and motility programs. *Nature Immunology* **14**, 41-51, doi:10.1038/ni.2477 (2013).

47 Iadecola, C. The Neurovascular Unit Coming of Age: A Journey through Neurovascular Coupling in Health and Disease. *Neuron* **96**, 17-42, doi:10.1016/j.neuron.2017.07.030 (2017).

48 Kumar, B., Connors, T. & Farber, D. Human T Cell Development, Localization, and Function throughout Life. *Immunity* **48**, 202-213, doi:10.1016/j.immuni.2018.01.007 (2018).

Figures

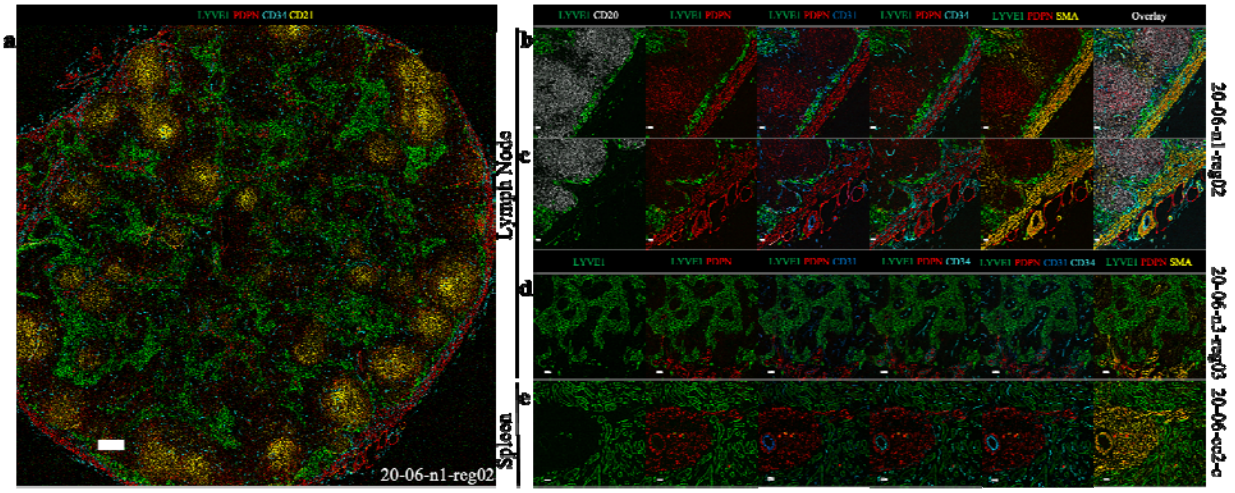

Figure 1. Lymphatic endothelial cell, blood vessel endothelial cell, and stromal cell organization in human LN and SPL. Representative CODEX images of **a-d**, LN and **e**, SPL. **a**, Cross-section of whole human LN showing the LEC markers, LYVE1 (green) and podoplanin (PDPN, red), BEC marker CD34 (cyan), and B cell marker CD21 (yellow). Scale bar, 750 µm. **b-c**, Within the LN, CD20+ (white) follicles lie adjacent to the floor of the subcapsular sinus expressing LYVE1 (green) and CD31 (blue), which is flanked on the opposite side by the ceiling of the subcapsular sinus expressing PDPN (red), CD34 (cyan), and smooth muscle actin (SMA, yellow); scale bars, 120 µm. **d**, LN medullary sinus expression of LEC markers (LYVE1 and PDPN), BEC markers (CD31 and CD34), as well as stromal cell marker, SMA. **e**, LYVE1 expression within SPL venous sinusoids, and PDPN and SMA expression surrounding trabecular arteries, identified by CD31 and CD34 expression. **d-e**, Scale bars, 180 µm. Donor ID, tissue, and region are defined **a**, in the bottom righthand corner and **b-e**, to the right.

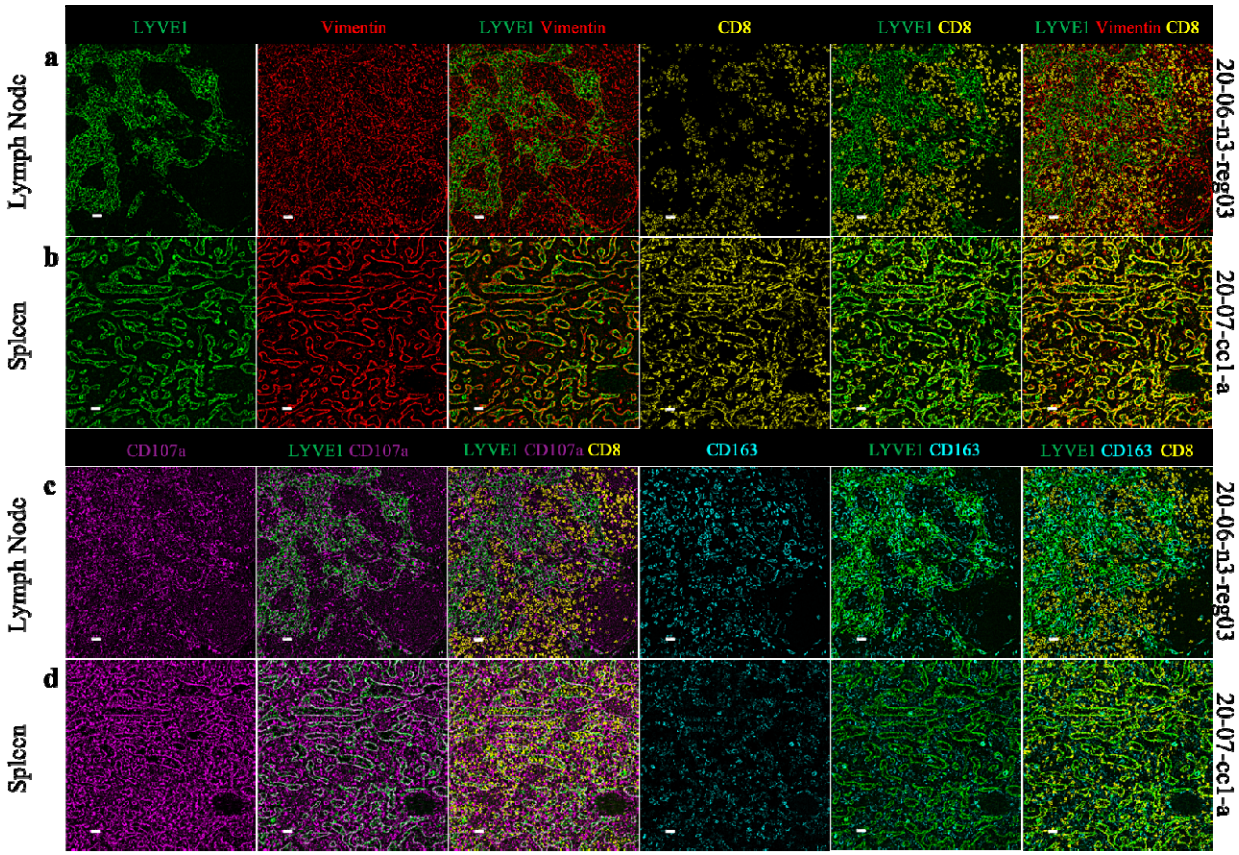

Figure 2. LYVE1 specifically labels the LN lymphatic conduit system and SPL venous sinuses. Representative CODEX images of human **a,c** LN medullary sinus and **b,d** SPL venous sinusoids, highlighting **a, b** LYVE1 (green), Vimentin (red), and CD8α (yellow) as well as **c,d** CD107a (purple), LYVE1 (green), CD8α (yellow), and CD163 (cyan). Scale bars, 120 µm. Donor ID, tissue, and region are defined to the right of each row.

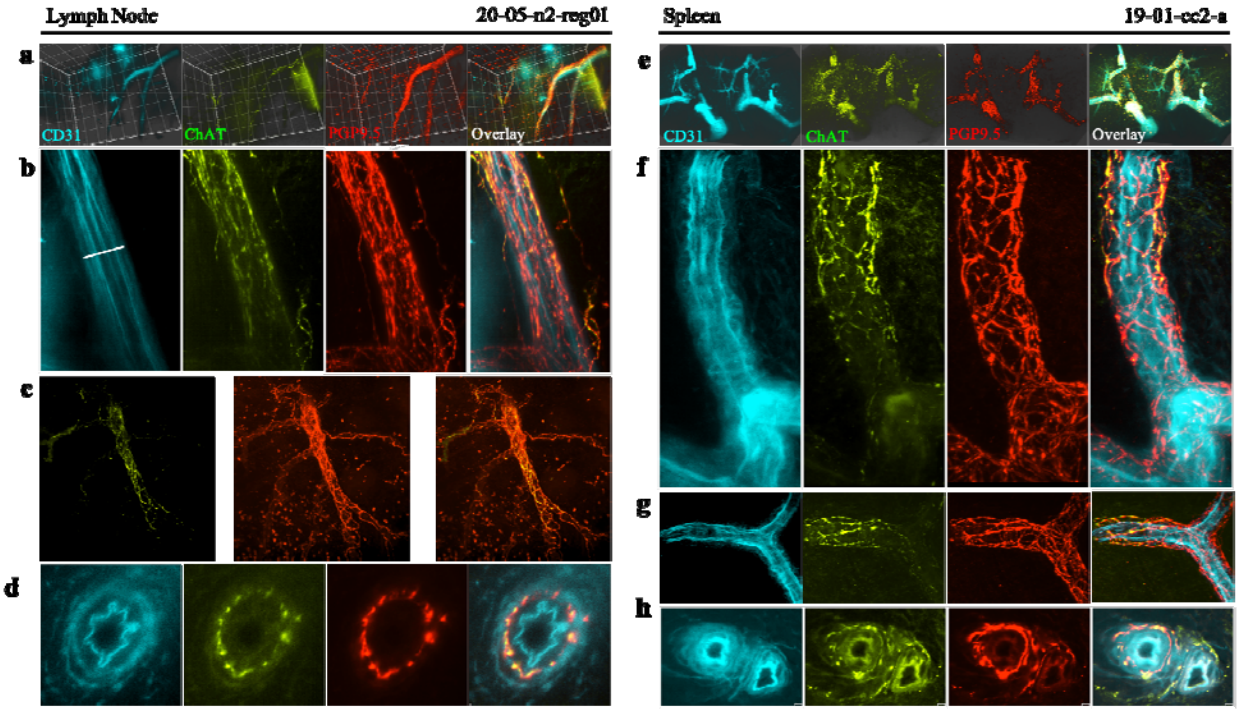

Figure 3. Perivascular innervation of human LN and SPL imaged with 3D LSFM. Multicolor LSFM imaging of CD31+ vessels (cyan) with ChAT (chartreuse) and PGP9.5 (red) innervation in **a-d**, LN and **e-h**, SPL. **a, e**, 3D rendering of 0.5-1 mm^3 tissue volumes. **b, f**, Max intensity projection of vessel expressing CD31 surrounded by extensive PGP9.5-positive innervation with partial ChAT-positive elements; scale bar, 100 µm. **c, g**, Wide-field max intensity projection of vessels with PGP9.5 perivascular innervation and partial ChAT innervation. **d, h**, Cross-section through vessels demonstrating co-localization of ChAT and PGP9.5 neural components within the *tunica externa*. Donor ID, tissue, and region are defined at the top.

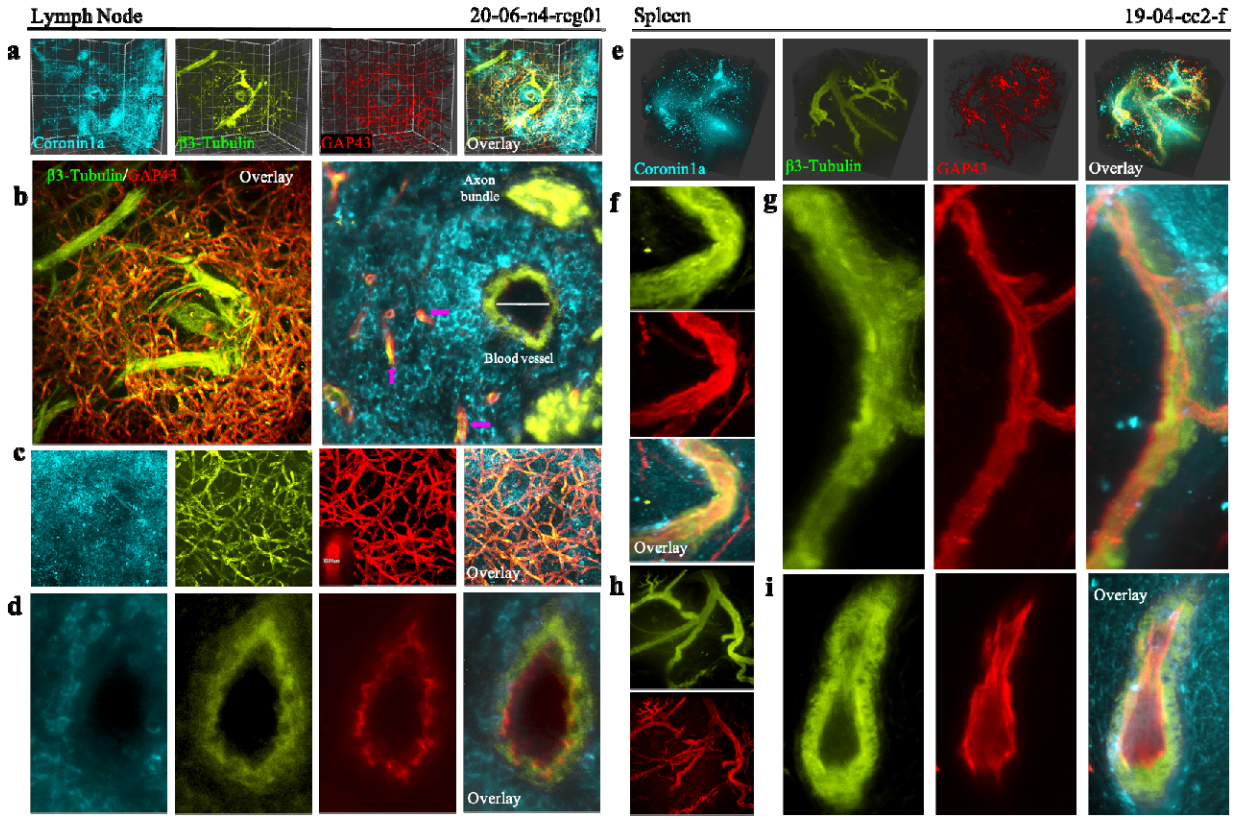

408

409 **Figure 4. Neural markers along ductal and vascular components of human LN and SPL.**
410 Multicolor LSFM imaging of Coronin-1A+ leukocytes (cyan) with β3-tubulin (chartreuse) and
411 GAP43 (red) innervation in **a-d**, LN and **e-i**, SPL. **a, e**, 3D rendering of 0.5-1 mm^3 LN tissue
412 volumes. **b**, Max intensity projection of LN vessel and nerve bundles expressing β3-tubulin
413 woven between an extensive GAP43-positive vessel network; scale bar, 60.5 µm. Pink arrows
414 indicate small vessels expressing GAP43 and β3-tubulin. **c**, Wide-field max intensity projection
415 showing Coronin-1A+ leukocytes among a complex network of β3-tubulin+ and GAP43+ small
416 diameter vessels; scale bar, 10.8 µm. **d,i**, Cross-section through vessels demonstrating
417 localization of β3-tubulin to the *tunica externa* and GAP43 to the *tunica interna* of the vascular
418 wall. **f-g**, Max intensity projection of SPL vessels expressing β3-tubulin within the wall and
419 GAP43 within the internal lining. Donor ID, tissue, and region are defined at the top.

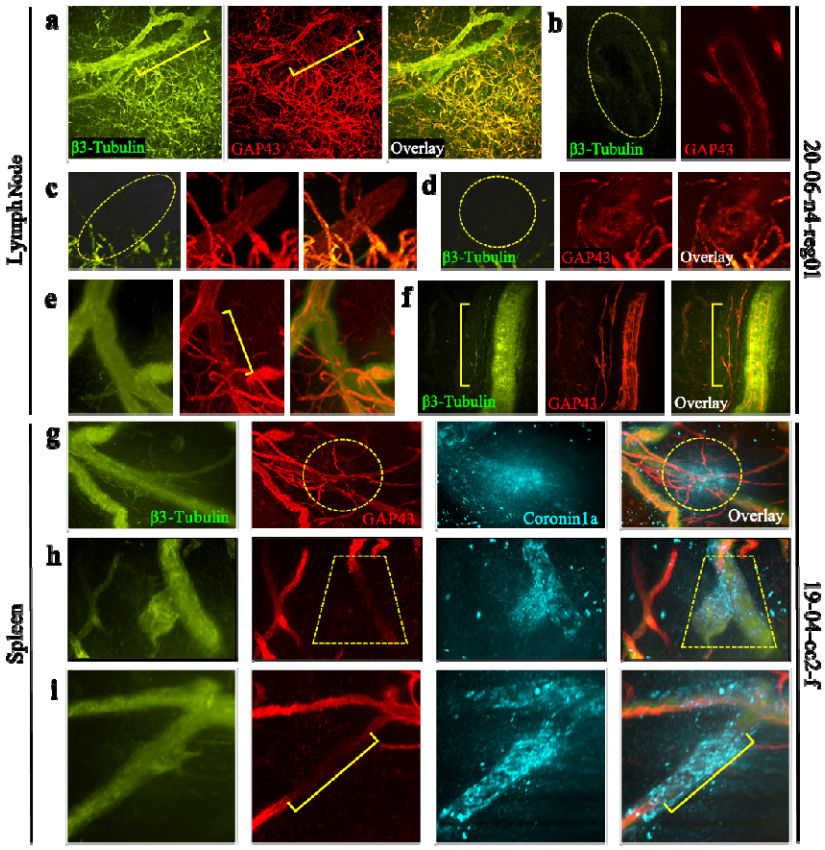

Figure 5. Differential expression of β3-tubulin and GAP43 along discrete segments large blood vessels in human LN and SPL. Multicolor LSFM imaging of β3-tubulin (chartreuse) and GAP43 (red) innervation with Coronin-1A+ leukocytes (cyan) in **a-f**, LN and **g-i**, SPL. **a**, Max intensity projection showing large β3-tubulin+ vascular segment with region of decreased GAP43 expression (yellow bracket). **b**, Cross-section of vessel demonstrating absence of β3-tubulin (dashed circle) where GAP43 expression is present. **c, d**, 3D renderings of 0.5-1 mm^3 LN showing two perspectives of GAP43+ vessel, absent β3-tubulin expression (dashed circles). **e**, Max intensity projection of vessel region with reduced GAP43 expression (yellow bracket). **f**, Max intensity projection of vessels showing reduced β3-tubulin expression on small diameter vessels where GAP43 is abundant (yellow bracket). **g-i**, Max intensity projection of SPL blood vessels showing region of continuous β3-tubulin, reduced GAP43, and concentrated Coronin1a expression (dashed outlines and yellow bracket). Donor ID, tissue, and region are defined to the right.

Methods

Donor Acceptance Criteria

Prior to organ recovery, written informed consent for research is provided by the donor families. Criteria for donor acceptance by the HuBMAP Lymphatic System TMC at the University of Florida are available on the HuBMAP site (https://www.protocols.io/view/donor-acceptance-criteria-for-tmc-florida-zurich-h-bipykdpw) and as follows: donors less than 7 days on a ventilator, tissue received within 24 hours of recovery, and donor body mass index (BMI) between the 5th and 95th percentile as defined by the United States Centers for Disease Control and Prevention (CDC). Contraindications for acceptance include: more than four blood transfusions, autoimmune disease, chromosomal abnormalities, positive culture for bacterial or viral meningitis, or methicillin-resistant *Staphylococcus aureus* (MRSA), sepsis, observable infarction, rupture, SLP or LN deflation or gross abnormality, immune deficiency disease, cancer, infection including severe acute respiratory syndrome-coronavirus-2 (SARS-CoV-2), and splenomegaly.

SPL and LN Case Processing and Quality Control (QC)

Human SPL and mesenteric LN were obtained from seven organ donors (Extended Data Table 1) and processed within 16 hours of cross clamp. Residual fat or connective tissues were removed from each LN and size (mm) recorded. LN > 1 cm^2 were bisected to 1 cm^2. LN < 1 cm^2 were left intact. Intact spleens were photo documented with hilum to left, inferior end at top. Cross-sectional slabs were cut 1 cm thick, and a 1 cm wide strip was cut through the center of each slab with the superior pole surface facing up and the hilum serving as the point of origin. 1 cm^3 blocks were dissected from each strip with all cuts photo documented for location and orientation. Tissue cassettes were placed in at least 20 volumes of 4% PFA (i.e., 20 mL 4% PFA per 1 mL tissue) for 20-24 hours, transferred to 70% ethanol, and paraffin embedded in an automated tissue processor (Sakura VIP) within 3 days. SPL and LN were sectioned to 5 µm

and stained with hematoxylin and eosin (H&E) and evaluated by an independent pathologist to assess organ normality.

Immunohistochemistry

IHC was performed according to HuBMAP Lymphatic System TMC standard operating procedures (SOPs) as detailed (https://www.protocols.io/view/dab-staining-of-ffpe-slides-bdiei4be). Formalin fixed, paraffin embedded (FFPE) human SPL and LN were sectioned to 5 μm, mounted on Superfrost Plus (Fisher Scientific) microscope slides and air dried overnight. Slides were deparaffinized twice in xylene and 100% ethanol for 5 minutes, peroxidase blocked with 3% peroxide in methanol for 10 minutes followed by serial ethanol washes (95%, 75% and 50%) each for 5 minutes. Finally, slides were washed in deionized water twice for 5 minutes. Antigen retrieval involved microwaving at 50% power for 7 minutes in 10 mM sodium citrate buffer pH 6.0 followed by an 18 minutes incubation in the hot citrate. Slides were then rehydrated with 50mM Tris buffered saline pH 7.6 with 0.1% Tween (TBST) for 5 minutes in a humidified chamber. Diaminobenzidine (DAB) staining was performed using VECTASTAIN Elite ABC Kit (peroxidase-HRP) kit (Vector Labs) and IMPACT DAB (peroxidase substrate). Avidin and biotin were sequentially blocked using Avidin/Biotin Blocking Kit (Vector Labs) for 20 minutes, followed by TBST rinse and incubation in 2% normal serum block (in TBST) for 1 hour. Primary antibodies were diluted in Antibody Diluent Reagent Solution (Life Technologies; Supplemental Table 1), applied to the slide, covered with a plastic coverslip and incubated overnight at 4°C in humidified chamber. Slides were incubated with diluted biotinylated secondary antibodies (5 μl antibody, 15 μl serum and 1 mL TBST) for 30 minutes at room temperature followed by addition of ABC Reagent for 30 minutes. Diluted DAB reagent was then added, development observed microscopically and reaction stopped in tap water. Slides were

then counterstained with hematoxylin followed by alcohol and xylene dehydration and cover-slipped.

CODEX Antibody Conjugation and Validation

Commercially available oligonucleotide conjugated antibodies were purchased from Akoya Biosciences and used at a standard dilution of 1/200 (Supplemental Table 1). Carrier-free purified antibodies for custom conjugation were validated by IHC in our lab using the tissues of interest (human SPL and LN). Conjugations were performed with commercially available CODEX Conjugation Kits (Akoya Biosciences) according the manufacturer's recommendation with the following modifications. Briefly, for each antibody, a 50 kDa molecular weight cut-off (MWCO) filter (Amicon Ultra) was washed with Filter Blocking Solution, centrifuged at 12,000 xg for 2 minutes and emptied of all liquid. To concentrate the antibody, 50 μg of protein, as determined by Nanodrop absorbance, was diluted in 100 μl PBS, added to the filter and centrifuged at 12,000 xg for 8 minutes. To initiate the disulfide reduction reaction, Antibody Reduction Master Mix was added to the filter, vortexed for 2-3 seconds, incubated at room temperature for no more than 25 minutes followed by buffer exchange. A unique barcode was prepared for each antibody (Supplemental Table 1) by reconstituting in 10 μl distilled water, adding 210 μl of the Conjugation Solution with incubation at room temperature for 2 hours. 5-10 μl of antibody solution was reserved for protein electrophoresis, and the filter washed three times with Purification Solution. Newly conjugated antibodies were collected by centrifugation. Custom conjugated antibodies were titrated (1/200, 1/100, 1/50) and validated by comparing the staining patterns of each conjugated antibody alone in CODEX against IHC DAB staining before being included in multiplex experiments. Newly conjugated antibodies were also stained alongside positive and negative controls in the CODEX platform as described (https://www.protocols.io/view/hubmap-tmc-uf-validation-of-custom-conjugated-anti-bkpzkvp6).

CODEX Staining and Imaging

Barcoded antibody staining of tissue sections mounted on cover slips was performed using a commercially available CODEX Staining Kit according to the manufacturer's instructions for FFPE tissue (Akoya Biosciences) and as recorded for HuBMAP Lymphatic System TMC SOPs (https://www.protocols.io/view/codex-antibody-staining-protocol-for-ffpe-tissues-bbsdina6). In brief, sample coverslips were heated to 55°C, cooled, deparaffinized and rehydrated. Antigen retrieval was performed using 1X Citrate pH 6.0 in a pressure cooker. Tissue coverslips were washed and equilibrated in CODEX Staining Buffer. Samples were incubated with barcoded antibodies (diluted as described in Supplemental Table 1) in CODEX blocking buffer for 3 hours in a humidity chamber at room temperature. After PBS washes, tissue sections were sequentially fixed with 1.6% paraformaldehyde (PFA), methanol (on ice) and Codex Fixative Reagent. Stained sample coverslips were stored for up to 2 weeks in CODEX Storage Buffer at 4°C. Barcoded fluorescent reporters corresponding to the barcoded primary antibodies were added to 96-well plates containing Codex Reporter Stock solution and nuclear stain, in groups of three (one of each wavelength) for each multiplex cycle (https://www.protocols.io/view/codex-preparation-of-reporter-96-well-plates-bc2riyd6). During cycling, the CODEX instrument automatically adds the reporter solution to the coverslip, acquires fluorescent images, removes the reporters (DMSO/1X CODEX Buffer wash), and prepares the tissue for the next cycle. Images were acquired at 20X magnification using a Keyence BZ-X810 microscope with a metal halide light source and filter cubes for DAPI (358), TRITC (550), CY5 (647) and CY7 (750). Typical images are 7x9 (3.77 x 3.58 mm) including acquisition of 17 Z-stack images at 1.5 µm pitch. Raw images were processed and stitched using CODEX Processor software including cycle alignment, drift compensation, background subtraction, and cell segmentation. Image analysis was performed with the Akoya Multiplex Analysis Viewer (MAV) in Fiji with KNN/FLANN clustering, gating and spatial network mapping.

Tissue Clearing

A CLARITY[49] based protocol was used to clear tissues. All incubation and wash steps were performed with gentle rocking. Samples (< 1 cm^3) were fixed in 40 mL of 4% PFA (Electron Microscopy Sciences) for 24 hours at 4°C, incubated for five days at 4°C in 40 mL of hydrogel monomer solution [4% acrylamide (Bio-Rad), 0.05% bis-acrylamide (Bio-Rad), 0.25% VA-044 Initiator (Wako Specialty Chemicals), 4% PFA, in PBS], then polymerized for 5 hours in 50 mL PBS at 37°C. Hydrogel embedded tissues were then cleared of lipids by incubating in 50 mL of clearing solution (Logos Bio) at 60°C, replacing clearing solution weekly until optically transparent. Cleared samples were washed in PBS with 0.1% Triton X-100 (PBST) for 48 hours at 37°C, replacing PBST wash buffer every 12 hours.

Immunolabeling and LSFM 3D Imaging

All incubation and wash steps were performed with gentle rocking. Cleared samples were immunolabeled by first incubating in 10 mL RTU Blocker and Diluent (Vector Laboratories) for 48 hours at room temperature. Primary antibodies (Supplemental Table 1) were diluted (1/200) in RTU Blocker and Diluent for 3 mL total volume added to samples, then incubated for five days at 37°C, then two days at 4°C. Samples were washed in 50 mL PBST at room temperature for five days, exchanging PBST wash buffer each day. Secondary antibodies (Supplemental Table 1) were diluted (1/200) in 5 mL RTU Blocker and Diluent, and samples were protected from light and incubated for five days at 37°C, then two days at 4°C. Samples were washed in 50 mL PBST at room temperature for five days, exchanging PBST wash buffer daily.

Immunolabeled samples were incubated in 20%, 40%, then 63% 2,2'-thiodiethanol (Sigma Aldrich) diluted with PBS at room temperature for two hours each to attain a refractive index of n = 1.45. Samples were then adhered to a glass capillary using cyanoacrylate to mount into the light sheet imaging chamber. Images were obtained with a Zeiss Z.1 Lightsheet

microscope using a 20x objective. Images were processed with Arivis Vision4D software (v.3.0.1) and are presented as single optical sections, max intensity projections, and 3D renderings.

Data availability statement

The data generated and/or analyzed during the current study are publicly available in the HuBMAP repository, https://portal.hubmapconsortium.org/search?entity_type[0]=Dataset.

Methods References

49. Chung, K. & Deisseroth, K. CLARITY for mapping the nervous system. *Nature Methods* **10**, 508-513, doi:10.1038/nmeth.2481 (2013).

Acknowledgements

We thank the families of the organ donors for the gift of tissues. This work was supported by a grant from the NIH NIAID (U54AI142766) to MAA, HSN, TMB, and CHW as well as (P01AI42288) to MAA, The Leona M. and Harry B. Helmsley Charitable Trust (G-2004-03813) to MAA, and JDRF (5-SRA-2018-557-Q-R) to MAA.

Author Contributions

SC, MJ, JAN, MAB, HH, and CHW performed the experiments and/or analyzed the data. MJ, MAB, JPA, NR, MMS, MY, IK contributed to donor organ acquisition and processing. SC, HSN, CHW, and MAA designed the research. HSN, KO, TMB, CHW, and MAA supervised the research. SC, HSN, and CHW integrated the data and interpreted the results. SC, HSN, CHW, ALP, and MAA wrote the manuscript. All authors discussed the results and edited the manuscript.

Competing Interest Declaration

The authors declare no competing interests.

Additional Information

Supplementary information is available for this paper.

Correspondence and requests for materials should be addressed to Mark A. Atkinson, PhD.

Extended Data Figure and Table Legends

Extended Data Table 1. Donor demographics, clinical information, and tissue sample identification numbers for SPL and LN examined by IHC, CODEX, and LSFM.

Extended Data Figure 1. Immunohistochemical assessment of immune, nervous, endothelial, and stromal markers in human LN and SPL. CD3ε, CD4, CD8α, CD20, CD21, CD15, Coronin-1A, CD31, CD34, Vimentin, CD107a, CD163, PGP9.5, β3-Tubulin, GAP43, ChAT, TH, LYVE1, PDPN and PROX1 were visualized by chromogen-based IHC in human LN (left) and SPL (right) to confirm anticipated staining pattern and determine appropriate antibody dilutions. DAB (brown) indicates a positive signal. Red arrows identify fine neural processes of PGP9.5 within insets of LN and SPL. Scale bars, 100 µm.

Extended Data Figure 2. Immune cell organization within human LN and SPL. CODEX images of **a**,**c**, LN and **b**,**d**, SPL illustrating immune cell distribution throughout tissue parenchyma. **a, b**, B cells are organized in follicles (CD20, yellow) among T cells (CD3ε, red), including cytotoxic (CD8α, green) and helper (CD4, blue) T cells in LN and SPL. **b**, CD8α+ LCs can also be visualized lining of the veinous sinusoids in the SPL. **c,d**, CD3ε (red) colocalizes with CD8α (green) or CD4 (blue) on T cells in LN and SPL. **d**, CD3ε-CD8α+ cells define the lining of the veinous sinusoids in the SPL. **c**, Granulocytes (CD15, cyan) and macrophages (CD68, purple) are distributed throughout LN cortex, though not as densely as T cells (CD3ε, CD4, CD8α). **d**, In SPL granulocytes (CD15) are concentrated around follicles and distributed throughout the red pulp. CD68+ macrophages are found primarily in the red pulp cords, interdigitated between the CD8α+ venous sinusoids. **a,c**, Scale bars, 950 µm. **b,d**, Scale bars, 750 µm. Donor ID, tissue, and region are defined to the right of each row.

Extended Data Figure 3. **Annotated LEC and BEC organization of LN capsule.** PDPN (red) and CD34 (cyan) are present in the ceiling of the LN subcapsular sinus, whereas LYVE1 (green) and CD31 (blue) are present within the floor of the subcapsular sinus and transverse sinus. An artery expressing CD31 surrounded by PDPN sits to the right of multiple lymphatic vessels outlined in with PDPN alone. Scale bar, 280 µm.

Extended Data Figure 4. LEC, BEC, and stromal cell organization in human LN. a-c, Representative CODEX images of LN from three different donors show CD20 (white), PDPN (red), CD31 (blue), CD34 (magenta), and SMA (yellow), scale bars, 120 µm. **a**, CD20+ follicles lie adjacent to the transverse sinus expressing LYVE1 and CD31, while PDPN, CD34, and SMA reside in the trabecula within the transverse sinus. **b**, LN region within the medullary sinuses encompassing a CD20+ follicles and multiple large vessels positive for PDPN, CD31, and SMA, surrounded by CD34. **c**, Regions of medullary sinus hosting multiple CD20+ follicles as well as a small vessel expressing CD31, CD34, PDPN, and SMA. **d**, Panels 1-5 show that LN cortical sinuses express LEC markers LYVE1 (green) and PROX1 (red), as well as the BEC marker CD31 (blue) and contain many granulocytes (CD15, yellow), scale bars, 180 µm. **d**, Within the far-right panel nucleus staining (DAPI, white) allow for clear visualization of the lumen within LYVE1+ sinus channels, scale bar, 40 µm. Donor ID, tissue, and region are defined to the right of each row.

Extended Data Figure 5. LEC, BEC, and stromal cell organization in human SPL. Representative CODEX images of SPL from two different donors show CD20+ (white) follicle surrounded by LYVE1+ (green) venous sinusoids, while trabeculae are highlighted by PDPN (red) and SMA (yellow). Central arteries of follicles can be identified by PDPN (red), CD31 (blue), and SMA (yellow) expression. Scale bars, 120 µm. Donor ID, tissue, and region are defined to the right of each row.

Extended Data Figure 6. LYVE1 specifically labels the LN lymphatic conduit system. Representative CODEX images of human LN medullary tissue from three different donors highlighting **a-c**, LYVE1 (green), Vimentin (red), and CD8α (yellow), as well as **d-f**, CD107a (purple) and CD163 (macrophages, cyan). Scale bars, 120 µm. Donor ID, tissue, and region are defined to the right of each row.

Extended Data Figure 7. LYVE1 specifically labels the venous sinuses in SPL. Representative CODEX images of human venous sinusoids in SPL from two different donors, denoted by **a-c** LYVE1 (green), stromal Vimentin (red), CD8α (yellow), and **d**, CD107a (purple). **d-f**, Panels demonstrating CD107a+ (purple) venous sinusoids and red pulp, while CD163+ macrophages (cyan) are found only within the red pulp. Scale bars, 120 µm. Donor ID, tissue, and region are defined to the right of each row.

Extended Data Figure 8. CD31 in SPL highlight endothelium and processes entering the *tunica media*. a, Max intensity projection (left) and single cross-section (right) of a CD31+ (cyan) blood vessel. **b**, Max intensity projection of blood vessel (CD31, cyan) spotted with nuclei (DAPI, white). **c**, 3D rendering of autofluorescent splenic blood vessel (cyan) ensheathed by neurons expressing tyrosine hydroxylase (TH, red). Vessel and neuronal network diameters are annotated on the figure and vessel cross-section overlay shown on the far right, emphasizing TH localization to the *tunica externa*. **d**, Cross-section of CD31+ (cyan) blood vessel annotated for internal and external vessel diameter, as well as perivascular PGP9.5 (red) innervation containing portions of ChAT+ (chartreuse) filaments. **e**, Cartoon depicting arterial architecture and location of neural elements with TH (red), β3-Tubulin (blue), PGP9.5 (green), and ChAT (yellow) localized to the *tunica externa* while GAP43 (light green) is localized within either the *tunica media* or *tunica intima* (created with BioRender.com).

Extended Data Figure 9. Multi-perspective 3D LSFM reveals masked phenomena. Front (upper row), top (middle), and side views (bottom row) of 3D rendering from human SPL stained for β3-tubulin (chartreuse) and GAP43 (red). Dashed cylinders highlight a β3-tubulin+ region of blood vessel where GAP43 expression is markedly reduced compared to proximal and distal GAP43 staining.